Rare Metal Materials and Engineering
Volume 48, Issue 12, December 2019
Available online at www.rmme.ac.cn

Science Press

Cite this article as: Rare Metal Materials and Engineering, 2019, 48(12): 3797-3805.

ARTICLE

Effect of Welding Speed on Microstructure Evolution and Mechanical Properties of 6005A-T5 Aluminum Alloy FSW Joints

Liu Jingxuan[1], Shen Jian[1,2], Li Xiwu[1], Yan Lizhen[1], Yan Hongwei[1], Liu Hongwei[1], Wen Kai[1], Li Zhihui[1], Zhang Yong'an[1], Xiong Baiqing[1,2]

[1] State Key Laboratory of Nonferrous Metals and Processes, GRIMAT Engineering Institute Co., Ltd, Beijing 101407, China; [2] GRINM Group Co., Ltd, Beijing 100088, China

Abstract: The 6005A-T5 aluminum alloy welded joints were prepared by friction stir welding (FSW) at different welding speeds. The microstructure and mechanical properties of these joints were investigated. The relationship between evolution of precipitates in different regions and mechanical properties of welded joints was established. The results show that β'' phases completely dissolve back into the aluminum matrix due to sufficient welding heat input in nugget zone (NZ) during the welding processing. GP zones form during the subsequent natural aging, which results in the hardness recovery of NZ. Incomplete recrystallization occurs in the thermo-mechanically affected zone (TMAZ), and the grains are elongated with high dislocation density. The heat affected zone (HAZ) contains Q' and β'' phases. With the decrease of welding speed, β'' phase gradually disappears and Q' phase forms, which leads to a decrease in the strength of welded joints. The average value of longitudinal residual stress is higher than that of transverse residual stress. With the increase of welding speed, the peak longitudinal residual tensile stress increases, but the effect on the transverse residual tensile stress is negligible.

Key words: aluminum alloy; friction stir welding; microstructure; mechanical properties; residual stress

Recently, the transportation industry has put forward higher requirements on lightweight materials. Al-Mg-Si alloys have received extensive attention due to their advantageous properties, such as low density, high strength-to-weight ratio, and excellent formability[1-3]. Al-Mg-Si alloys are usually used in high-speed train as sidewalls and roofs of train bodies to reduce the weight and associated fuel consumption[1,4,5]. Therefore, the application of welding technology is necessary. Traditional fusion welding technology is always accompanied by some defects, such as pores, solid impurities and hot cracks[6-10]. These defects seriously damage the mechanical properties and service life of welded joints. This issue can be effectively solved by friction stir welding (FSW), which is a solid state welding method[11]. Since the welding metal of FSW does not undergo fusion and solidification, a series of metallurgical problems associated with it can be avoided[12].

Precipitation hardening is the major strengthening mechanism in the Al-Mg-Si alloys[13,14]. The precipitation sequence of Al-Mg-Si alloys is usually as follows[2,15]: SSSS →solute clusters→GP zones→β''→β'→β, where SSSS is the supersaturated solid solution. In Cu-contained alloys, the precipitation process is much more complicated. The precipitation sequence is generally reported as[16,17]: SSSS→ solute clusters→GP zones→β''→β', Q'→Q. Solute clusters are aggregates of highly concentrated solute atoms[18]. GP zones are formed by ordered arrangements of a larger number of solute on Al lattice positions[17]. The solute clusters and GP zones are spherical, which can provide nucleation position for β'' phases during further aging. The β'' phase is generally considered as the main hardening phase. The β' and Q' phases

Received date: December 23, 2018
Foundation item: National Key R&D Program of China (2016YFB0300905, 2016YFB0300902)
Corresponding author: Shen Jian, Ph. D., Professor, GRINM Group Co., Ltd, Beijing 100088, P. R. China, Tel: 0086-10-60662809, E-mail: shenjianpaper@126.com

are formed under overaging, where Q' is considered as the precursor of Q and has orderly hexagonal crystal structure[19-21]. All precipitates have different effects on the strength of materials. The evolution of precipitated phases occurs in FSW joints due to thermal cycling during welding. However, the degree of welding heat input depends on welding parameters. Different welding parameters change the precipitation behavior of welded joints. Accordingly, the mechanical properties of welded joints also change. Sato et al[22] researched the precipitation-hardenable behavior of 6063-T5 alloy FSW joint. They found that no precipitates exist in the nugget zone, so the nugget zone shows the lowest Vickers hardness compared with other regions. Dong et al[23] showed that β' and Q' phases appear in the HAZ of 6005A-T6 FSW joint instead of β'' phases. They also found that the length of precipitated phase increases and the number density decreases with the increase of welding speed.

It is generally acknowledged that friction stir welded joints have good mechanical properties. However, residual stress usually affects the application of welded joints and deteriorates the performance of welded joints in service. Many researchers have studied the residual stress in welded joints. Steuwer et al[24] studied the residual stress of AA5083-AA6082 dissimilar FSW welded joints. They reported that the distribution curve of residual stress is close to the welded zone, presenting "M" shape, and the peak residual stress appears near the tool shoulder position. Lombard et al[25] have examined the residual stress of AA5083-H321 FSW joint by synchronous X-ray radiation. They showed that there is a linear relationship between the peak residual stress and heat input. Moreover, the heat input is dominated by the welding speed and peak residual stress increases with the increase of welding speed.

In this paper, ~6 mm 6005A-T5 aluminum alloy was welded by friction stir welding at different welding speeds. The effect of welding speed on microstructure and mechanical properties of welded joint was discussed. In addition, the residual stress of welded joints was tested. It is expected to provide a basis for the study of how to regulate residual stress by welding parameters.

1 Experiment

1.1 Material and welding parameters

The 6005A-T5 aluminum alloy was used as the base material (BM) for the present investigation, and the chemical composition is presented in Table 1. The dimension of 6005A-T5 sheets is 350 mm×150 mm×6.5 mm.

Before welding, all plates were cleaned by picking and degreasing to remove the oxidation layer and oil stains. FSW was performed using a tool with a shoulder diameter of 18 mm and a pin diameter of 6.2 mm. The detailed welding parameters are listed in Table 2. All welding plates were placed at room temperature for more than four weeks before subsequent tests.

Table 1 Chemical composition of 6005A-T5 alloy base material (wt%)

Mg	Si	Cu	Fe	Mn	Cr	Zn	Al
0.58	0.68	0.13	0.16	0.24	0.11	0.01	Bal.

Table 2 Welding parameters of FSW

Rotational speed/r·min^{-1}	Welding speed/mm·min^{-1}
1500	100
1500	500
1500	900

1.2 Residual stress and performance test

The residual stresses were measured on a Pulstec μ-X360s X-ray residual stress analyzer. This technique uses a single tilt angle and measures distortion in the complete Debye ring formed from diffraction by the {311} planes[26]. The transmission depth of the diffractometer was about 10 μm and the irradiated area was approximately a disc with 2 mm in diameter. The standard Cr target was selected as target material. The test points were 3 mm apart, and the longitudinal stress and transverse stress were measured at each point.

Vickers hardness of the joints was measured by a 430SVD Vickers hardness tester, according to the standard ASTM: E384, with a loading of 3 kg for 10 s dwell time. The hardness test was performed in the transverse cross-section at 1 mm intervals. To ensure that the weld zone was at the center of the tensile samples, the specimen was prepared according to ASTM standard E517-00 with the tensile direction perpendicular to the welding direction. Tensile tests were performed by a WD3100 test machine at room temperature with a constant rate of 1 mm/min.

1.3 Microstructure characterization

The different microstructure characteristics of the samples were analyzed by optical metallography (OM), electron back-scattering diffraction (EBSD) and transmission electron microscope (TEM). All specimens were cut by an electrical discharge cutting machine.

The metallographic samples were burnished and polished, and then treated with Keller's reagent for approximately 60 s. The samples for EBSD test were burnished and polished, followed by electropolishing test in a solution (10 mL $HClO_4$+ 90 mL C_2H_5OH) for 6~8 s at a voltage of 25 V and a current of 0.5~1 A. The precipitates were characterized by TEM examinations (TecnaiG2 F20 microscope). Different regions of samples were mechanically ground to a thickness of 50~60 μm, and then these slices were prepared by double-jet electropolishing in a solution (25% nitric acid and 75% methanol) at about −30 °C and 15~25 V.

2 Results and Discussion

2.1 Macrostructure observation

Fig.1 shows the surface appearance of friction stir welded joint group at welding speeds of 100, 500 and 900 mm/min and

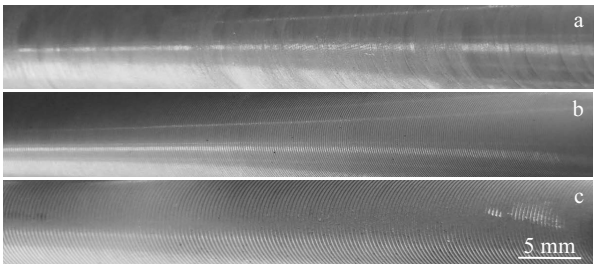

Fig.1 Surface appearance of FSW joint group with the welding speeds of 100 mm/min (a), 500 mm/min (b) and 900 mm/min (c) at a constant rotation speed of 1500 r/min

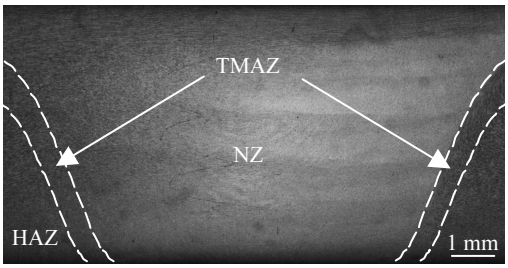

Fig.2 Cross-section macrograph of FSW joint at rotation speed of 1500 r/min and welding speeds of 100 mm/min

a constant rotation speed of 1500 r/min. Smooth and defect-free welded joints can be obtained by these three sets of welding speeds. It can be seen that a series of arc crest and arc trough form. The spacing of arc crest increases with the increase of welding speed.

According to the structure characteristics, the FSW joints consist of four parts: the nugget zone (NZ), the thermo-mechanically affected zone (TMAZ), the heat affected zone (HAZ) and the base material (BM). Fig.2 displays the cross-sections morphology of the joints at rotation speed of 1500 r/min and welding speeds of 100 mm/min. The shape of the nugget zone can be seen clearly. The boundary of NZ on advancing side (AS) is more explicit than on retreating side (RS). Meanwhile, the onion rings can be observed in the center of NZ.

2.2 Microstructure characteristics

2.2.1 Grain morphology analysis

Fig.3 shows the grain morphology of NZ and HAZ in welded joints at different welding speeds. The grain size of NZ is smaller than that of BM due to dynamic recrystallization. It can be clearly seen from Fig.3a~3c that the grain size of NZ varies greatly with welding speeds. Whereas, the difference of grain size in HAZ is not significant (Fig.3d~3f). As shown in Fig.4, the average grain size of NZ is decreased from 19.9 μm to 13.4 μm as the welding speed increases from 100 mm/min to 900 mm/min. This is due to the increase of cooling rate with the increase of welding speed. However, the maximum grain size of HAZ is 31.2 μm and the minimum is 29.5 μm at different welding speeds. It should be noted that the peak temperature of HAZ is much lower than that of NZ, which results in a small change gap of grain size.

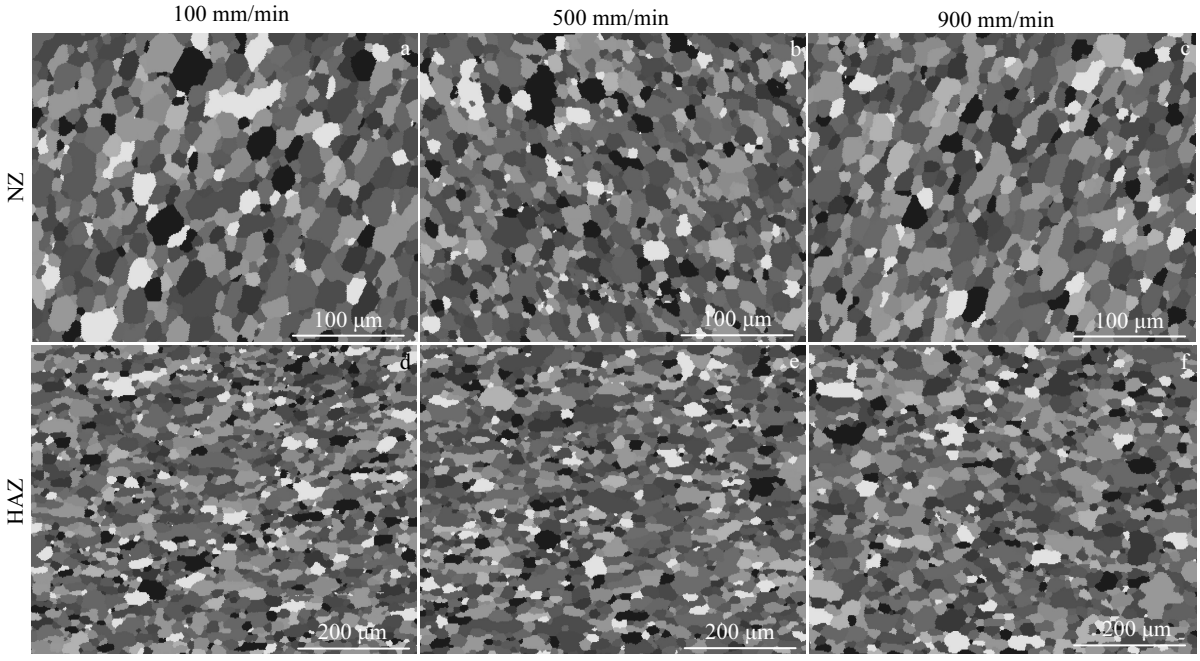

Fig.3 EBSD map of 6005A-T5 aluminum alloy FSW joints at different welding speeds

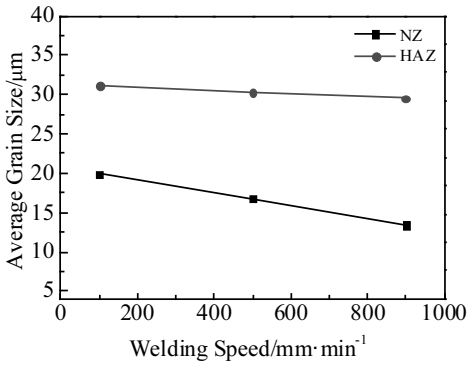

Fig.4 Average grain size of welded joints at different welding speeds

2.2.2 TEM observation of precipitates

Fig.5 shows TEM bright field images of base material (BM). The needle-shaped precipitates lie in the <001>$_{Al}$ direction and are uniformly distributed in the Al matrix, which can be clearly observed in the bright field image (Fig.5a). The precipitates are 20~50 nm in length and ~10 nm in radius. A cross-shaped diffraction streak is displayed in the corresponding selected area electron diffraction (SAED) pattern, as shown in Fig.5b. Besides, the HRTEM image and corresponding fast Fourier transform (FFT) pattern confirm that these phase particles are β" phase[16, 27]. As shown in Fig.5c, the embedded β" phase has a monoclinic structure, its long axis is parallel to <$\bar{3}$20>$_{Al}$ and the short axis is aligned to <130>$_{Al}$. It is worth mentioning that the needle-like β" phases are the major hardening precipitates of BM.

Fig.6 shows TEM bright field images and corresponding SAED patterns of different regions at different welding speeds. In the nugget zones (NZs), there is no sign of β" phase except for some fine phases. Moreover, the corresponding SAED patterns reveal only the diffraction spots of Al matrix. Previous studies[28] have reported that the dissolution temperatures of β" phases are ranged from 200 °C to 250 °C. Nevertheless, the peak temperature of NZ in FSW joints usually exceeds 500 °C[23]. The results indicate that all the original β" phases dissolve irrespective of welding speed. Fig.7 shows the HRTEM image and corresponding FFT pattern of the fine phases. The phases, which are spherical with 1~3 nm in size, are completely coherent with Al matrix. Meanwhile, there is no additional information in the corresponding FFT pattern. Thus, these fine phases are identified as GP zones[29]. Supersaturated solid solution (SSSS) is formed when NZ is subjected to high heat input and fast cooling rate. This leads to the formation of solute clusters during nature aging. With the increase of nature aging time, the GP zones gradually evolve from solute clusters. Since the size of solute clusters is too small, only GP zones can be observed in bright field images.

The structure of TMAZ is not only affected by heat input, but also by plastic deformation. As shown in Fig.8, a large number of dislocations with a network structure are observed

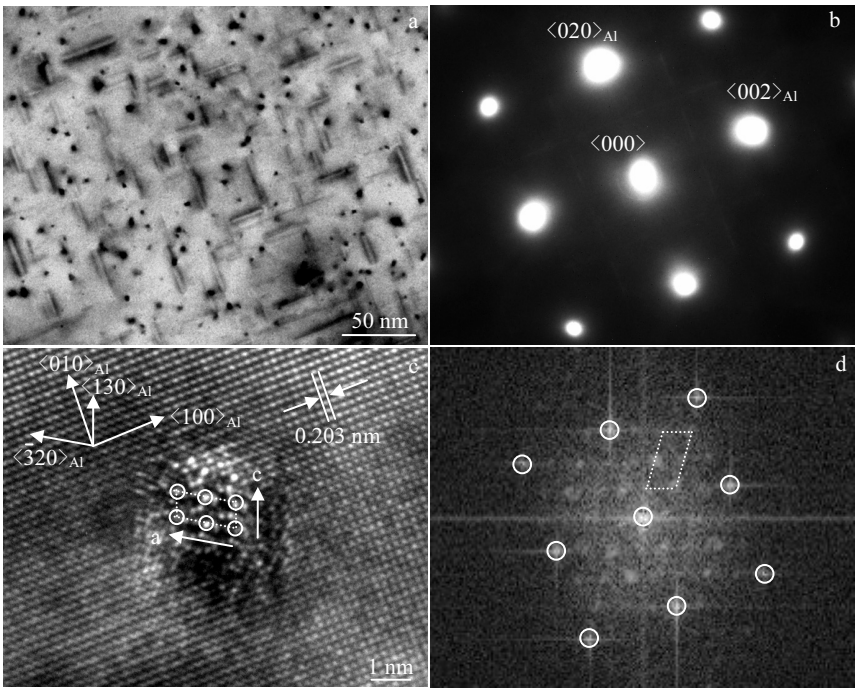

Fig.5 TEM images of 6005A-T5 aluminum alloy: (a) bright-field image, (b) SAED pattern, (c) HRTEM image of β" phase, and (d) corresponding FFT pattern

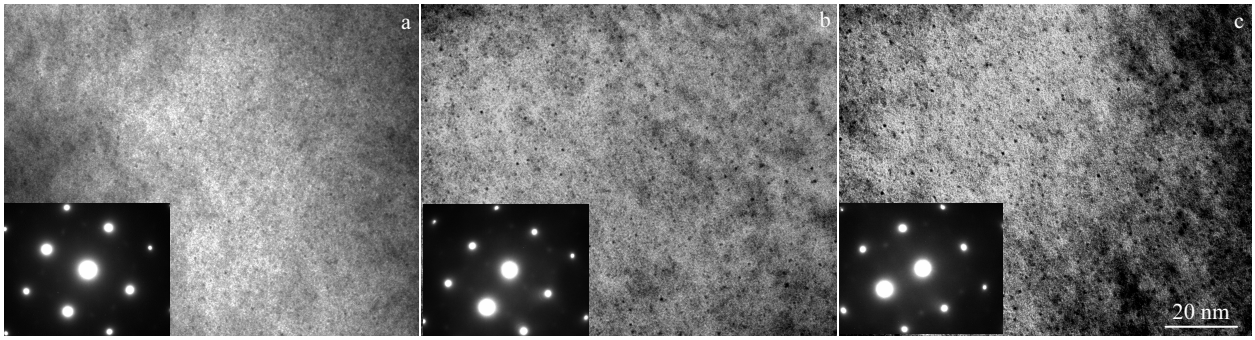

Fig.6 TEM images and <001>$_{Al}$ SAED patterns of NZ at the welding speeds of 100 mm/min (a), 500 mm/min (b), and 900 mm/min (c)

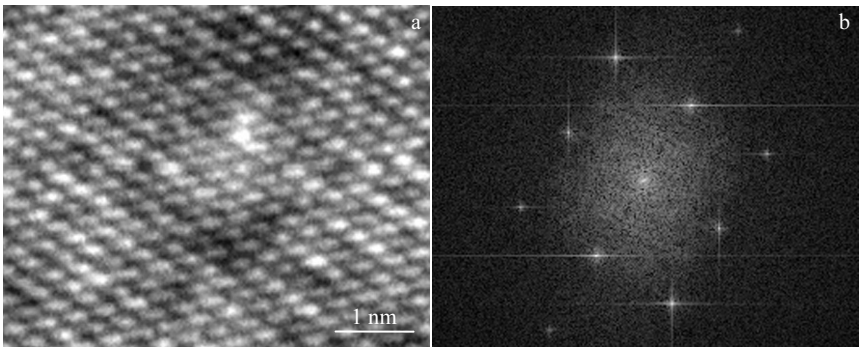

Fig.7 HRTEM image (a) and corresponding FFT pattern (b) of GP zone

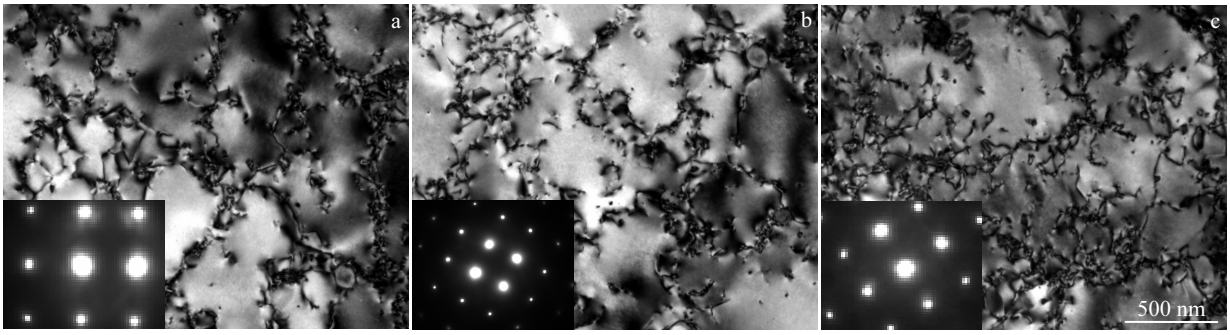

Fig.8 TEM images and <001>$_{Al}$ SAED patterns of TMAZ at the welding speeds of 100 mm/min (a), 500 mm/min (b), and 900 mm/min (c)

in TMAZ. The peak temperature of TMAZ is second only to that of NZ, so there are no visible precipitates in this region. The result is also reflected in corresponding SAED patterns. This phenomenon is similar to NZ.

Fig.9 shows TEM bright field images and corresponding SAED patterns of HAZ at various welding speeds. Welding speed has a significant effect on the type, size and distribution of precipitate phases, which can be clearly observed from Fig.9. Fig.9a shows the morphology and distribution of precipitate phases at a low welding speed (100 mm/min). There is only one type of lath-like precipitate phases. Fig.10 shows the HRTEM image and corresponding FFT pattern of the lath-like precipitate. It has orderly hexagonal crystal structure with a cross-section elongated along <510>$_{Al}$. Therefore, the lath-like precipitates are identified as Q' phases[17]. It is generally believed that Q' phase is transformed from β'' phase[30]. At a relatively high speed (500 mm/min), the dimension of Q' phase decreases significantly and its number density increases markedly. Interestingly, a small amount of needle-like β'' phases can be observed in Fig.9b.

This indicates that the welding heat input of HAZ at this speed is insufficient for all the β'' phases to transform into Q' phases. At a high welding speed (900 mm/min), most β'' phases and a few Q' phases are observed in Fig.9c. Compared with the β'' phases in Fig.9b, the β'' phases in Fig.9c have a smaller size and a larger quantity density due to the lower peak temperature in HAZ.

2.3 Joint properties

Vickers hardness was measured along mid-thickness line of transverse cross-section of the samples to obtain the distribution curves of hardness at various welding speeds. Fig.11 shows the effect of welding speeds on the hardness distribution. It can be observed that all the hardness curves of FSW joints exhibit a typical "W" shape. The hardness curves are almost symmetric with respect to the weld line. The slight difference is related to the non-uniformity of material flow on the both sides of welded joints. There is a distinct softening zone in all welded joints. The average hardness of NZ, TMAZ and HAZ is much lower than that of BM (1000 MPa). The minimum hardness appears in the HAZ due to dissolution of β'' phases and coarsening of Q' phases, which are shown in Fig.9. Furthermore, the width of softening zone decreases and the minimum hardness of softening zone increases with the increase of welding speed. The increase of welding speed means the decrease of heat input during the welding process. Hence, β'' phases do not have enough driving force to dissolve or transform into Q' phases. The average hardness of NZ is higher than that of HAZ. It is related to the formation of solute clusters or GP zones in NZ during natural aging, which can be clearly observed in TEM images (Fig.6). In addition, the

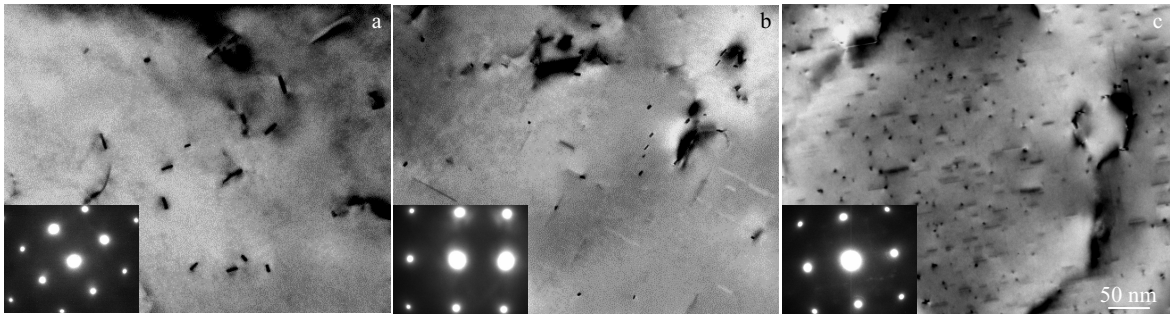

Fig.9 TEM images and <001>$_{Al}$ SAED patterns of HAZ at the welding speeds of 100 mm/min (a), 500 mm/min (b), and 900 mm/min (c)

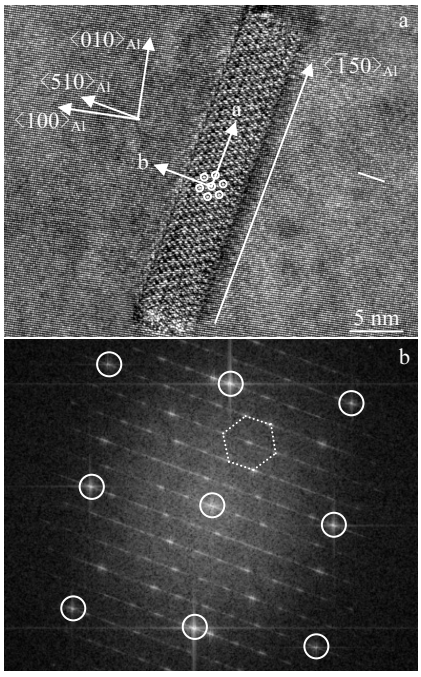

Fig.10 HRTEM image (a) and corresponding FFT pattern (b) of Q' phase

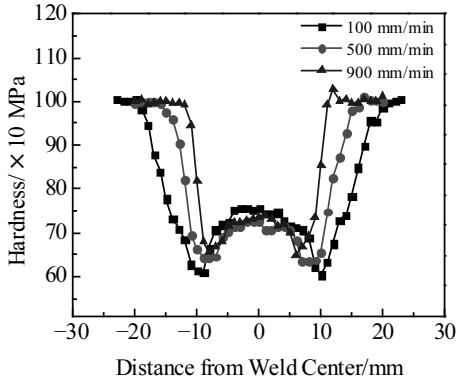

Fig.11 Hardness profiles of FSW joints at different welding speeds

grains of NZ are refined during welding processing, so the effect of refined crystalline strengthening cannot be neglected. The average hardness of NZ decreases with the increase of welding speed. This indicates that more heat input means the matrix having more energy for reprecipitation. The average hardness of TMAZ is slightly lower than that of NZ. The degree of reprecipitation in TMAZ is weaker than in NZ on account of the less heat put, although a mass of dislocations can be observed in this region (Fig.8), and the dislocations can

contribute to hardness.

Fig.12 shows the effect of welding speed on the tensile properties of welded joints. It is obvious that the tensile properties of all welded joints decrease compared to those of BM. At a constant rotation speed of 1500 r/min, ultimate tensile strength (UTS) and yield strength (YS) have an upward tendency with the increase of welding speed from 100 mm/min to 900 mm/min, but elongation (EL) shows an opposite case. The welding efficiency (ratio of UTS of the joint to UTS of BM) of welded joints increases from 71.5% to 82.0%. All fractures occur in HAZ near TMAZ on advancing side. From the hardness distribution curve in Fig.11, the fracture location is consistent with the position of the minimum hardness. This indicates that the tensile properties of welded joints major depend on the microstructure of HAZ. In other words, the tensile properties of welded joints are dominated by the evolution of precipitate phases in HAZ.

2.4 Residual stress

Fig.13 shows the distribution of longitudinal and transverse residual stresses in welded joints at various welding speeds. The measurement range of residual stress is 40 mm from the center of weld zone. As shown in Fig.13a, it can be seen that the profile of residual stress in longitudinal direction is shown as an "M" shape. This result is in good agreement with previous reports in Ref.[24]. The longitudinal residual stress in the region around weld center is mainly the tensile stress and the balancing compressive stress in base material. The residual stress ranges from −57 MPa to 178 MPa at different welding speeds. Peak residual stress measurements are located next to the tool shoulder. However, it is worth noting that the position of peak residual stress is gradually away from the tool shoulder as the welding speed decreases. The peak stresses are located at 14, 12 and 10 mm from the weld center at the welding speed of 100, 500 and 900 mm/min, respectively. The distribution of residual stress on both sides of the weld center is not completely symmetrical. The peak residual stress in advancing side is slightly higher than in retreating side. This result is contrary to the conclusion reported by Zapata et al[31]. They measured the residual stresses of AA2024-T3 and AA6061-T6 alloys and found that all the maximum residual stresses of welded joints are located on the retreating side. There is a sharp decline of residual stress in NZ compared with near the tool shoulder. The minimum residual stress in NZ of welded joint is only 29 MPa at the welding speed of 100 mm/min. The width of tensile stress seems to be extremely sensitive to the variation of welding speed. With the increase of welding speed, the width of tensile stress remarkably decreases.

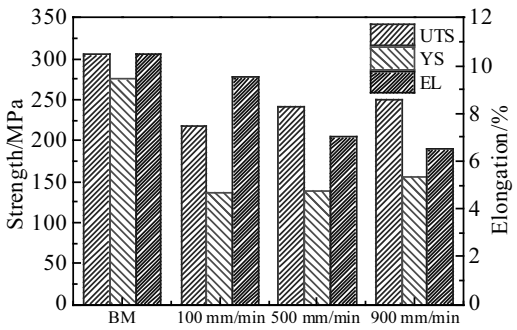

Fig.12 Tensile properties of FSW joints at different welding speeds

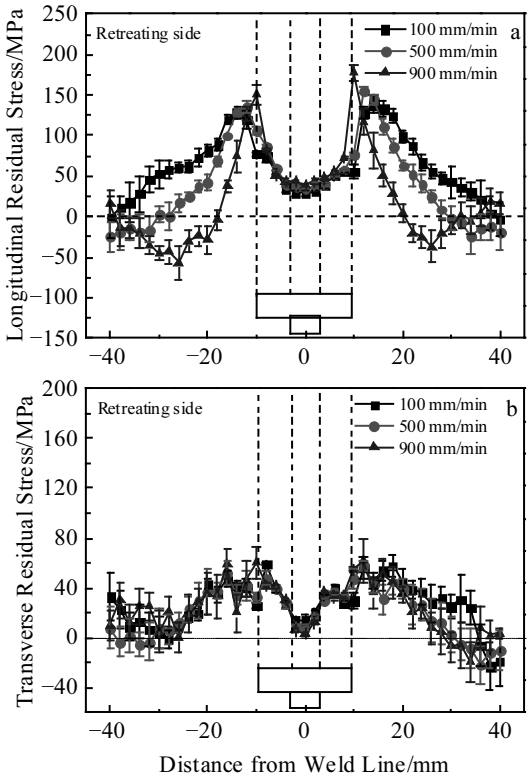

Fig.13 Longitudinal (a) and transverse (b) residual stress distribution of FSW joints at different welding speeds

The average value of transverse residual stresses is much lower than that of longitudinal residual stress, as shown in Fig.13b. The maximum tensile stress value is just 62 MPa. The distribution curves of transverse residual stress at different welding speeds present a good consistency, which implies that transverse stress is slightly affected by welding speed.

Fig.14 shows peak longitudinal residual stress and width of longitudinal tensile stress at different welding speeds. It exhibits that the trend of residual stress varies with welding speed. It is clear that the peak stress increases from 128 MPa to 182 MPa with the increase of welding speed, but the width of tensile region is inversely proportional to welding speed. Welding speed determines heat input per unit length. Higher heat input can spread farther away from weld center, thereby affecting thermal expansion mismatch upon cooling.

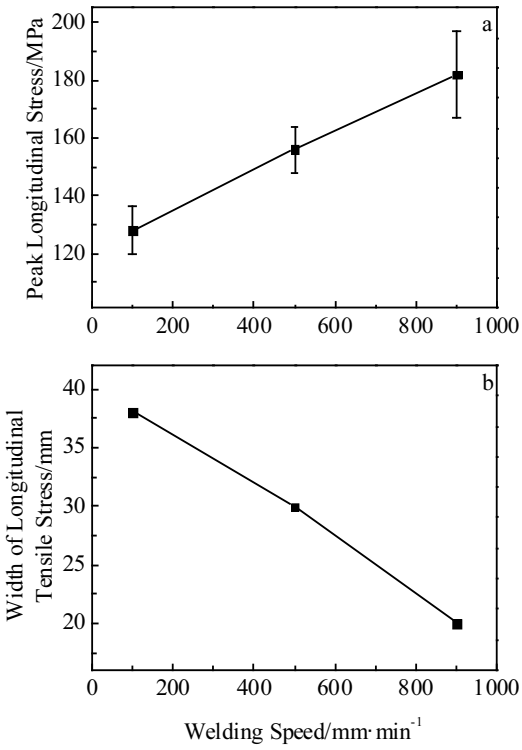

Fig.14 Peak longitudinal residual stress (a) and width of longitudinal tensile stress (b) of FSW joints at different welding speeds

3 Conclusions

1) The NZ shows a fine grain structure due to dynamic recrystallization. The average grain size of NZ and HAZ decreases with the increase of welding speed. The HAZ is not subjected to mechanical stir of the tool, so the grain morphology has no significant change.

2) The NZ experiences the highest temperature, β" phases dissolve back into the Al-matrix and GP zones are precipitated subsequently during natural aging. The number of β" phase decreases and Q' phases are coarsened in HAZ with the decrease of welding speed.

3) Tensile strength and yield strength of FSW joints increase with increasing the welding speed, while elongation decreases slightly. The welding efficiency of welded joints ranges from 71.5% to 82.0%.

4) The residual stress of the weld region is generally tensile stress and the balancing compressive stress in BM. The average value of longitudinal residual stress in weld region is larger than that of transverse residual stress. Peak residual stress increases with the increase of welding speed.

References

1 Williams, James C, Starke *et al*. *Acta Materialia*[J], 2003, 51(19): 5775

2 Edwards G A, Stiller K, Dunlop G L *et al*. *Acta Materialia*[J], 1998, 46(11): 3893

3 Pogatscher S, Antrekowitsch H, Leitner H *et al*. *Acta Materialia*[J], 2011, 59(9): 3352

4 Dong P, Sun D, Li H. *Materials Science and Engineering A*[J], 2013, 576: 29

5 Miller W S, Zhuang L, Bottema J *et al*. *Materials Science and Engineering A*[J], 2000, 280(1): 37

6 Yan Z, Liu X, Fang H. *The International Journal of Advanced Manufacturing Technology*[J], 2017, 91(9): 3025

7 Da Silva C L M, Scotti A. *Journal of Materials Processing Technology*[J], 2006, 171(3): 366

8 Gou G, Zhang M, Chen H *et al*. *Materials & Design*[J], 2015, 85: 309

9 Wang X, Mao S, Chen P *et al*. *Materials & Design*[J], 2016, 90: 230

10 Liu H, Zhao Y, Hu Y *et al*. *The International Journal of Advanced Manufacturing Technology*[J], 2015, 78(9): 1415

11 Mishra R S, Ma Z Y. *Materials Science and Engineering*[J], 2005, 50(1): 1

12 Nandan R, DebRoy T, Bhadeshia H K D H. *Progress in Materials Science*[J], 2008, 53(6): 980

13 Zhu S, Li Z, Yan L *et al*. *Journal of Alloys and Compounds*[J], 2019, 773: 496

14 Zhu S, Li Z, Yan L *et al*. *Materials Characterization*[J], 2018, 145: 258

15 Huis M A V, Chen J H, Zandbergen H W *et al*. *Acta Materialia*[J], 2006, 54(11): 2945

16 Yang W, Wang M, Jia Y *et al*. *Metallurgical and Materials Transactions A*[J], 2011, 42(9): 2917

17 Torsæter M, Lefebvre W, Marioara C D *et al*. *Scripta Materialia*[J], 2011, 64(9): 817

18 Fallah V, Langelier B, Ofori-Opoku N *et al*. *Acta Materialia*[J], 2016, 103: 290

19 Ravi C, Wolverton C. *Acta Materialia*[J], 2004, 52(14): 4213

20 Marioara C D, Andersen S J, Stene T N *et al*. *Philosophical Magazine*[J], 2007, 87(23): 3358

21 Chakrabarti D J, Laughlin D E. *Progress in Materials Science*[J], 2004, 49(3): 389

22 Sato Y S, Urata M, Kokawa H. *Metallurgical and Materials Transactions A*[J], 2002, 33(3): 625

23 Dong P, Li H, Sun D *et al*. *Materials & Design*[J], 2013, 45: 524

24 Steuwer A, Peel M J, Withers P J. *Materials Science and Engineering A*[J], 2006, 441(1-2): 187

25 Lombard H, Hattingh D G, Steuwer A *et al*. *Materials Science and Engineering A*[J], 2009, 501(1-2): 119

26 Tanner D A, Robinson J S. *Materials Science and Technology*[J], 2016, 32(14): 1533

27 Andersen S J, Zandbergen H W, Jansen J *et al*. *Acta Materialia*[J], 1998, 46(9): 3283

28 Gaber A, Ali A M, Matsuda K *et al*. *Journal of Alloys and Compounds*[J], 2007, 432(1): 149

29 Liu S, Li K, Lu J *et al*. *Journal of Alloys and Compounds*[J],

2018, 745: 644
30 Ding L, Jia Z, Nie J F *et al*. *Acta Materialia*[J], 2018, 145: 437
31 Zapata J, Toro M, López D. *Journal of Materials Processing Technology*[J], 2016, 229: 121

焊接速度对 6005A-T5 铝合金搅拌摩擦焊接头组织演变及力学性能的影响

刘敬萱[1]，沈　健[1,2]，李锡武[1]，闫丽珍[1]，闫宏伟[1]，刘红伟[1]，温　凯[1]，李志辉[1]，张永安[1]，熊柏青[1,2]
(1. 有研工程技术研究院有限公司 有色金属材料制备加工国家重点实验室，北京 101407)
(2. 有研科技集团有限公司，北京 100088)

摘　要：采用不同焊接速度对 6005A-T5 铝合金进行搅拌摩擦焊，对其焊接接头的组织和力学性能进行研究。建立了不同焊接接头区域析出相的演变和力学性能之间的关系。在焊接的过程中，焊核区由于受到了足够的热输入，β''相完全回溶到铝基体。在后续的自然时效过程中逐渐形成 GP 区，这也是焊核区硬度上升的主要原因。热影响区发生不完全再结晶，晶粒呈现拉长状，同时有大量的位错形成。热影响区主要包含 Q'相和 β''相。当焊接速度下降时，焊接接头的强度随着 β''相的回溶和 Q'相的形成逐渐降低。焊接接头纵向残余应力的平均值要大于横向残余应力。当焊接速度增加，纵向残余应力的峰值随之增加，但对横向残余应力的影响可以忽略。

关键词：铝合金；搅拌摩擦焊；组织；力学性能；残余应力

作者简介：刘敬萱，男，1990 年生，博士，有研工程技术研究院有限公司，有色金属材料制备加工国家重点实验室，北京 101407，电话：010-60662656，E-mail: liujingxuan90@126.com